INNOVATIVE MECHANICAL ENGINEERING **ISSN 2812-9229 (Online)**
University of Niš, Faculty of Mechanical Engineering
VOL. 2, NO 1, 2023, PP. 13 - 22

Original scientific paper *

PERFORATED PLATE CONVECTIVE HEAT TRANSFER COEFFICIENT DETERMINATION

Mladen Tomić[1], Predrag Živković[2], Biljana Prochaska[3], Miroslav Kljajić[1], Borivoj Stepanov[1]

[1] University of Novi Sad, Faculty of Technical Sciences

[2] University of Niš, Faculty of Mechanical Engineering

[3] University of Banja Luka Faculty of Mechanical Engineering

Abstract. *Numerical simulations were performed to calculate the heat transfer coefficient of a perforated plate with cylindrical perforations arranged in a square pattern. The study varied three parameters: plate porosity (ranging from 0.1 to 0.3), Reynolds number (based on pitch) and the working fluid (air, carbon dioxide, or water). Perforation diameter and plate thickness were held constant. The Reynolds number was varied between 200 and 3000 for air and carbon dioxide, and between 500 and 7000 for water. The simulation results were presented in the form of Nu=f(Re·Pr) and compared with an empirical correlation for perforated plates with low porosity.*

Key words: *Heat transfer, Perforated plate, Pitch, Porosity, Working fluid*

1. INTRODUCTION

One of the key characteristics of heat exchangers, in addition to high efficiency, is compactness. This means that they have a high surface area to volume ratio, which helps to control heat exchange with the surroundings by reducing exposed surface area. A small mass also results in a smaller cooling load and faster cooling time for refrigeration. This is particularly important for small refrigerators that operate at liquid helium temperatures. Various types of cryogenic heat exchangers have been reviewed in literature [1].

The need for both high efficiency and compactness led to the development of matrix heat exchangerinins (MHE) by McMation et al. [2]. These heat exchangers consist of a package of

*Received: January 21, 2023 / Accepted: February 01, 2023.
Corresponding author: Mladen Tomić
University of Novi Sad, Faculty of Technical Sciences
e-mail: mladen.tomic@uns.ac.rs

perforated plates with multiple flow passages aligned in the direction of flow, allowing for high heat transfer in a properly designed unit. They can have up to 6000 m^2/m^3 surface-to-volume density [3]. The entire package, along with cast aluminum headers at each end, is held together by steel tie rods. Neoprene spacers nearly eliminate axial conduction and provide gas-tight seals even at liquid air temperatures. The construction is simple and repairs are easy. Full-scale commercial units were intended for use in liquid oxygen production.

In 1966, an extensive experimental study of convective heat transfer and flow friction using transient techniques was published for eight different perforated surfaces [4]. The authors concluded that the perforations of perforated plate heat exchangers disturb the thermal boundary layer to a greater extent than the hydrodynamic boundary layer. They also found that by using perforated materials, an improvement in heat transfer can be achieved. A thorough literature review can be found in the papers of G. Venkatarathnam and Ragab M. Moheisen's report [5,6].

Based on the above, perforated plates and fins have found a wide range of applications in different heat exchangers, film cooling, and solar collectors [7-12]. The goal of this study is to determine the heat transfer coefficient for a 2 mm thin square-arranged perforated plate. The porosity was varied from 0.1 to 0.3 and the Reynolds number was between 200 and 5000, while the hole diameter was kept constant.

2. HEAT TRANSFER COEFFICIENTS REVIEW

The heat transfer improvement may generally be achieved by increasing the heat transfer coefficient, heat transfer surface areas, or both. In the papers [13-15] authors have concluded that for certain perforation sizes, perforated plate enhances heat transfer compared to the solid one. Perforated plate convective heat transfer takes place on three surfaces: front area surface, the tubular surface of a perforation and the back surface of the plate section. The flow through the tubular section could be considered as developing flow with the very high heat transfer coefficient. Heat transfer coefficient in the developing flow is well studied, and it can be calculated as the function of Peclet number [16]:

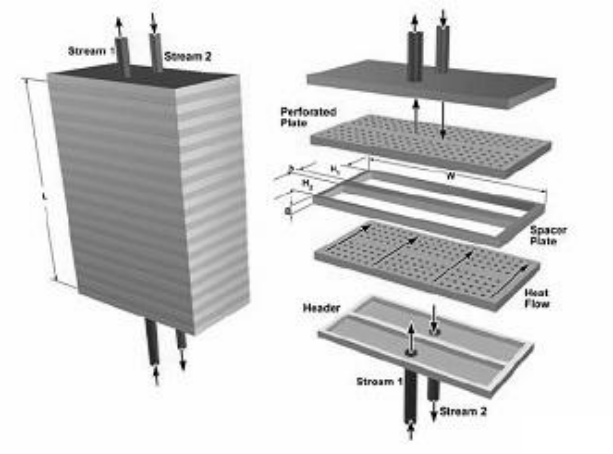

Fig. 1 Matrix heat exchanger schematic

$$\alpha = \zeta \cdot 0.0465 \cdot Pe^{0.75} \frac{\lambda}{d}. \quad (1)$$

where ζ is a function of the pipe length L and a length of pipe needed for developed flow L'. The length L' is equal to

$$L' = 0.015 \cdot Pe \cdot d. \quad (2)$$

Value Pe represents the Peclet number, as the function of Reynolds and Prandtl number, and d is the pipe diameter. The values for ζ are presented in the Table 1.

Table 1 The values of ζ

L/L`	0	0.01	0.05	0.1	0.2	0.4	0.6	0.8	1.0	∞
ζ	∞	1.26	1.16	1.12	1.08	1.05	1.03	1.01	1.00	1.00

Linghui et al. [17] have studied a flow through hexagonally arranged perforations. The purpose of the research was to determine how the length-to-diameter ratio (δ/d) of the plate's holes affects the heat transfer coefficient. They studied ratios varying from 0.333 to 1.1666, holding the diameter constant while thickness was varied. Their experiments used the naphthalene sublimation technique to determine the plate heat transfer. The research led to the conclusion that there was little change in the heat transfer coefficients between the (δ/d) ratios of 0.5 and 1.1. The final equation for the Nusselt number inside the tube was

$$Nu = 2.058 \cdot Re^{0.487}. \quad (3)$$

The heat transfer from the front face of the plate has been studied by Sparrow and Ortiz [18]. In their experiments Reynold's number per hole and the hole`s pitch-to-diameter ratio were varied. The suggested Nusselt criteria are function of the Reynolds and Prandtl number, but the characteristic length in the Nusselt criteria was the ratio of module surface area to the pitch:

$$Nu = 0.881 \cdot Re^{0.476} \cdot Pr^{1/3}, \ 2000<\text{Re}<20000, \quad (4)$$

and

$$Nu = \frac{\alpha \cdot A}{\lambda \cdot p}. \quad (5)$$

The result was established for the limited case, where the relative pitch is 2<p/d<2.5. Dorignac et al. [19] have conducted a series of experiments of airflow leading to the result for Reynolds number of 1000 to 1200:

$$Nu = 1.202 \cdot \left(\frac{p}{\sqrt{A}}\right)^{1.879} \cdot \left(\frac{p}{d}\right)^{0.163} \cdot Re^{0.409}, \quad (6)$$

where p is the pitch length and A the active surface. Similarly, the proposed definitions of the Reynolds number are based area to pitch ratio as in the Eq. (5).

Heat transfer rate in the back face of the last plate is high due to flow separation and resulting turbulence [20]. Brunger et al. [21] studied the effectiveness for each of the three zones of heat transfer on a perforated plate: the front of the plate, the inside of the tube, and the back of the plate. In their study, they considered large pitch to diameter ratios (> 6.67).

For each of the heat transfer regions, an equation for effectiveness was given. The authors also stated that under typical operating conditions, about 62% of the ultimate temperature rise of the air was predicted to occur on the front surface, 28% in the hole, and 10% on the back of the plate. An average heat transfer for the plate may be defined as:

$$\alpha = \frac{\sum_{i=1}^{n} \alpha_i \cdot A_i}{\sum_{i=1}^{n} A_i}. \tag{7}$$

Nusselt number correlated as a function of the Reynolds number, Prandtl number, and geometry factors is generally applicable to higher Reynolds numbers and lower plate porosities. Most of the authors have derived empirical correlations for the Nusselt number and friction factor versus the Reynolds number. The general approach was to find a relationship in the form:

$$Nu = \mathrm{C} \cdot Re^{n}, \tag{8}$$

where *C* and *n* are functions of the geometric parameters. Reynolds number is usually based on the flow velocity in the perforation and its diameter as a characteristic length. A good review of these functions could be found at [3, 5, 6]. A study for low-Reynolds-number flows (Re≤100) over a range of geometric parameters, including plate open-area ratio and hole diameter-to-plate thickness ratio was done by Rodriguez [22].

Andrew et al. [23] developed a model to determine the convective heat transfer coefficient of the upstream face, tube walls, and the leeward face of a perforated plate using computational fluid dynamics (CFD). The plate's holes were modeled as hexagonally shaped flow patterns, which corresponds to Sparrow's [20] model presented earlier. The data obtained from the CFD model were found to agree within a few percent of Sparrow's data. This led to their conclusion that the CFD model and solution were valid. A final equation for the Nusselt number, for $2000 \leq Re \leq 20000$ for the front side of a perforated plate was presented as:

$$Nu = 1.057 \cdot Re^{0.457} \cdot Pr^{0.333}. \tag{9}$$

where *C* and *n* are functions of the geometric parameters. Reynolds number is usually based on the flow velocity in the perforation and its diameter as a characteristic length. A good review of these functions could be found at [3, 5, 6]. A study for low-Reynolds-number flows (Re≤100) over a range of geometric parameters, including plate open-area ratio and hole diameter-to-plate thickness ratio was done by Rodriguez [22].

The model was applied to the tube surface of the perforations and the leeward side of the perforated plate to study their effect on the overall convective heat transfer coefficient of the matrix heat exchanger. This showed that the plate thickness had a substantial influence on the amount of heat transfer occurring within the tube part of a matrix heat exchanger, and that the leeward side of the perforated plate requires more investigation. In conclusion, an equation for the Nusselt number as a function of the Reynolds number was presented, considering the convection of the front, the back, and the tube of the perforation hole, considering air as a working fluid (Pr=0.7):

$$Nu = 0.397 \cdot Re^{0.652}. \tag{10}$$

Kutscher [24] conducted experiments to evaluate the overall convective heat transfer process for unglazed transpired solar collectors subjected to uniform approaching flow. Unglazed transpired solar collectors (UTCs) consist of dark porous cladding installed as

the exterior layer of the building envelope (normally roof or façade) with a narrow gap beneath it. The cladding absorbs solar radiation, thus heating the air flowing through the perforations driven by a suction fan. The following empirical correlation was obtained for a low-porosity plate for the average *Nu* of the entire plate surface:

$$Nu = 2.75 \cdot \left(\left(\frac{p}{d} \right)^{-1.2} \cdot Re^{0.43} + 0.011 \cdot \sigma \cdot Re \cdot \left(\frac{w}{v} \right)^{0.48} \right), \tag{11}$$

where p is the pitch length, d is the hole diameter, v is the suction velocity. Reynolds number was based on the suction velocity and hole diameter. In the case of the flow through a perforated plate, the equation reduces to:

$$Nu = 2.75 \cdot \left(\left(\frac{p}{d} \right)^{-1.2} \cdot Re^{0.43} \right), \tag{12}$$

where the Reynolds number is based on the free stream velocity and hole diameter. The *Nu* criteria in the equation is for low porosity plates, but the Nusselt number defined in terms of the heat transfer coefficient is based on the log mean temperature difference. The plate thickness in the experiment was 0.794 mm and according to Kutscher [24] it does not have a significant influence.

3. Mathematical and Numerical Model

In order to choose the best suitable model, several of the k-ε variants were tested: standard k-ε model, low-RE k-ε, RNG k-ε and k-ω model. Althrough all of them gave similar results, the RNG k-ε model (Tab. 2) presented itself as the fastest convergenting, and therefore was adopted for the simulation. In the study, a plate with 16 x16 perforations was placed in the numerical channel (Fig. 2). The mathematical model is based on the:

Continuity equation

$$\frac{\partial(\rho)}{\partial t} + \frac{\partial}{\partial x_i}(\rho \cdot u_i) = 0 \tag{13}$$

Momentum (Navier – Stokes) equations

$$\frac{\partial(\rho \cdot u_i)}{\partial t} + \frac{\partial}{\partial x_j}\left(\rho \cdot u_i \cdot u_j\right) = \frac{\partial}{\partial x_j}\left(\tau_{ij}\right) - \frac{\partial p}{\partial x_i} + f_i \tag{14}$$

Energy equation

$$\frac{\partial(\rho \cdot h)}{\partial t} + \frac{\partial}{\partial x_i}(\rho \cdot u_i \cdot h) = \frac{\partial}{\partial x_i}(j_{ih}) + S_h \tag{15}$$

where ρ is the density, u_i are the three main velocity components, p is the pressure, f_i are the body forces and any additional momentum sources, h is the enthalpy and S_h represents the generation/destruction rate of enthalpy. The τ_{ij} is the momentum shear stress tensor and the j_{ih} is the diffusion flux of energy transport.

In the energy equation, the diffusion flux of the energy transport term j_{ih} includes the energy transfer due to conduction, species diffusion and viscous dissipation:

$$j_{ih} = \Gamma_T \frac{\partial h}{\partial x_i} - \sum_j h_j \cdot j_{jc} + \Phi \tag{16}$$

where the factors Γ_T are the diffusion coefficients for the enthalpy (Fourier's law). The second term of the right side of the Eq. (5) represents the energy transport by diffusion of species and the Soret-effect diffusion transport respectively. Finally, the term Φ is the viscous dissipation defined as:

$$\Phi = 0.5 \cdot \mu \cdot \left(\frac{\partial u_i}{\partial x_j} + \frac{\partial u_j}{\partial x_i}\right)^2 - \frac{2}{3} \cdot \mu \cdot \frac{\partial u_k}{\partial x_k} \frac{\partial u_l}{\partial x_l}, \tag{17}$$

As the former equations represent the system averaged equations, it was needed to implement a turbulent model in order to close the system and to convert the given set of differential equations into algebraic, which were solved using the PHOENICS software package. The details are given in the following table:

Table 2 RNG k-ε turbulent model transport equations and constants

Transport equation	Φ	Γ_Φ	S_Φ
Turbulent kinetic energy	k	ν_t/σ_k	$\rho\,(G - \varepsilon)$
Turbulent kinetic energy dissipation	ε	ν_t/σ_ε	$\rho\,(\varepsilon / k)(C_{\varepsilon 1}G - C_{\varepsilon 2}\varepsilon)$
$G = \nu_t\,(\partial_k U_i + \partial_i U_k)\,\partial_k U_i$		$\nu_t = C_\mu k^2 / \varepsilon$	
$(\sigma_k\,,\ \sigma_\varepsilon\,,\ C_{\varepsilon 1}\,,\ C_{\varepsilon 2}\,,\ C_\mu) = (0.7194,\ 0.7194,\ 1.42,\ 1.68,\ 0.0845)$			

The plate was set to be a constant temperature heat source. The fluid stream was set to flow perpendicularly to the plate.

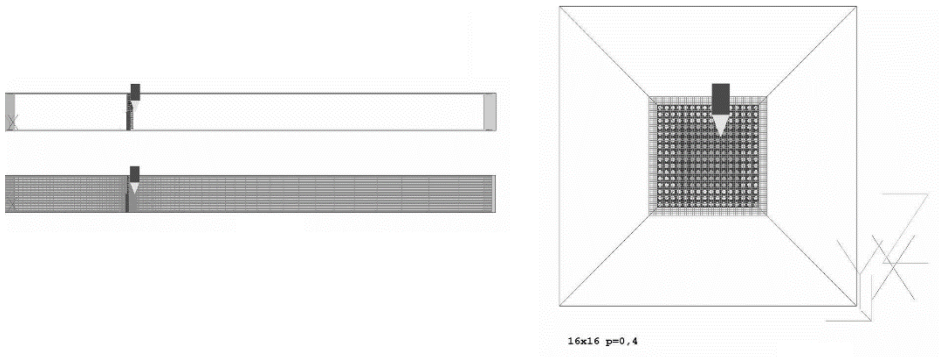

Fig. 2 Side (left) and front view (right) of the numerical channel with the grid

Table 3 Outlet temperature variation as function of the cell length

Cell edge size [mm]	Outlet temperature [°C]
0.878	21.65
0.798	22.30
0.721	22.28
0.598	22.33
0.527	22.35
0.351	22.22
0.263	22.40

To generate the optimal grid, the grid size was varied in two directions along plate length and width, regarding the Y - Z plane, so that the size of the cell edge was mutually equal (Fig.2). The cell edge length was varied from 0.88 to 0.2 mm and the fluid temperature on the outlet was chosen as a quality parameter. The results have shown that under the size of 0.8 mm, the temperature on the outlet was varying not more than 0.1K (Table 3). According to this, the cell length was chosen to be 0.5 mm, *i.e.*, 4 cells per hole diameter. The energy balance for the fluid side reads:

$$\dot{Q} = \dot{m} \cdot c_p \cdot \Delta t, \tag{18}$$

i.e.

$$\dot{Q} = \rho \cdot w \cdot S \cdot c_p \cdot (t_{out} - t_L), \tag{19}$$

where c_p represents mass specific heat capacity and w is the fluid velocity.

On the other hand the heat taken from the plate is equal to:

$$\dot{Q} = \alpha \cdot A \cdot \Delta\theta, \tag{20}$$

i.e.

$$\dot{Q} = \alpha \cdot A \cdot (t_{pl} - t_L), \tag{21}$$

where F represents the active heat transfer surface, and $\Delta\Theta$ iz the differnce between plate surface temperature and inlet fluid temperature. Combining Eqs. (19) and (21), heat transfer coefficient equals to:

$$\alpha = \frac{\rho \cdot w \cdot S \cdot c_p \cdot (t_{out} - t_{in})}{F \cdot (t_{pl} - t_L)}. \tag{22}$$

4. Results And Discussion

For the Nusselt criteria an arbitrary function was chosen in the form:

$$Nu = f(Re), \tag{23}$$

where Reynolds number is defined as the free stream fluid velocity function per hole pitch:

$$Re = \frac{w \cdot p}{\nu}, \tag{24}$$

and the Nusselt number is equal to:

$$Nu = \frac{\alpha \cdot p}{\lambda}. \quad (25)$$

The final forms of the Nusselt criteria have been presented in Fig. (3) and Tab. (4).

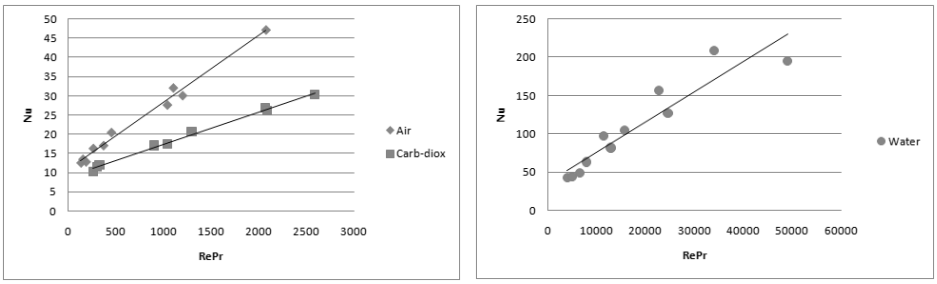

Fig. 3 Nusselt number dependency for different fluids

Table 4 Nusselt number dependency for different fluids

Fluid	Reynolds number range	Nusselt criteria	R^2
Air	200-3000	0.0174·RePr+10.95	0.987
Carbon-dioxide	200-3000	0.0084·RePr+8.98	0.994
Water	500-7000	0.0396·RePr+36.96	0.875

According to [24] for the low porosity plate, under the value of 5%, the Nusselt number for air flow is equal to:

$$Nu = 2.75 \cdot \left(\left(\frac{p}{d} \right)^{-1.2} \cdot Re^{0.43} \right), \quad (26)$$

where *Re* number is based on the free stream velocity and hole diameter. The Nusselt criteria in the Eq. (26) is defined in terms of the heat transfer coefficient based on logarithm mean temperature difference. The hole diameter was varied from 0.8 to 2 mm. Reynolds number was varied from 200 to 3000, and the maximal error was 12.5%.

5. CONCLUSION

The results presented in this paper shows that perforated plate convective heat exchange depends strongly on the porosity of the plate. The dependences proposed in the literature are not adequate for square arranged perforated plate, or were established for a specifically constructed equipment, or limited parameters t. In this paper a Nusselt criteria was obtained for wider range of parameters, when porosity is in the range 0.1 to 0.3. The error analysis has presented that criterial equation could be efficiently used for thin plates in the range of diameters from 0.8 to 2 mm. Compared with other criterial equations developed for low-porosity perforated plates and compared with simulated results, it could be concluded that obtained Nusselt relations are adequate for usage for the mentioned porous plate.

Nomenclature

Latin alphabet

A - active area, [m^2]
C - constant, [-]
c_p - specific heat capacity for constant pressure, [$J \cdot kg^{-1} \cdot K^{-1}$]
d - diameter, [m]
h - specific enthalpy, [$J \cdot kg^{-1}$]
i - coordinate, [-]
j coordinate, [-]
L - lenght, [m]
$\dot{m}$ - mass flow, [$kg \cdot s^{-1}$]
p - pitch size, [m]
S - flow corss section area, [m^2]
t - temperature, [°C]
w - fluid velocity, [$m \cdot s^{-1}$]

Greek alphabet

α - heat transfer coeffcient, [$W \cdot m^{-2} \cdot K^{-1}$]
λ - thermal conductivity, [$W \cdot m^{-1}\ K^{-1}$]
μ - dynamic viscosity, [Pa·s]
ν - kinematic viscosity, [$m^2 \cdot s^{-1}$]
ρ - density, [$kg \cdot m^{-3}$]
σ - porosity, [-]
θ - temperature difference, [K]

REFERENCES

1. Bogdan C., Brill C., Sirosh O, *et al.*, 2021, *Preliminary development of a conceptual model of matrix heat exchanger*, Smart Energy and Sustainable Environment, 24 (1), pp. 29-40.
2. McMahon H., O., Bowen R. J., Bleye G. A. JR, 1950, *A perforated plate heat exchanger*, Transactions of ASME 72, pp. 623-632.
3. Krishnakumar K., Venkataratham G., 2003, *Transient testing of perforated plate matrix heat exchangers*, Cryogenics, 43 (2), pp. 101-109.
4. Bannon J.M., Piersall C.H. Jr., Pucci P.F., 1965, *Heat transfer and flow friction characteristics of perforated nickel plate-fin type heat transfer surfaces*, Technical report no. 52, United States naval Postgraduate School, p. 116.
5. Venkataratham G., Sarangi S., 1990, *Matrix heat exchangers and their application in cryogenic system*, Cryogenics, 30 (11), pp. 907-918.
6. Ragab M.M., 2009, *Transport phenomena in fluid dynamics: Matrix heat exchangers and their applications in energy systems*, Report No. Afrl-rx-ty-tr-2010-0053, Air force research laboratory materials and manufacturing directorate, p. 24.
7. Kakac S., Bergles A.E., Mayinger F., 1981, Heat Exchangers, Thermal- Hydraulic Fundamentals and Design, Hemisphere Publishing Corporation, p. 1131.
8. Bergles A.E., 1981, *Technique to augment heat transfer*, In Handbook of heat transfer Applications, (Edited by Werren M. Rohsenow, James P. Hartnett, and Ejup N. Ganic), Ch. 3, Second Edition, McGraw-Hill Book company, NY.
9. Al-Essa A.H., AL-Hussien F.M.S., 2004, *The effect of orientation of square perforations on the heat transfer enhancement from a fin subjected to natural convection*, Heat and Mass Transfer, 40 (6-7), pp. 509-515.

10. Mullisen R., Loehrke R., 1986, *A study of flow mechanisms responsible for heat transfer enhancement in interrupted-plate heat exchangers*, Journal of Heat Transfer (Transactions of the ASME), 108 (2), pp. 377-385.
11. Kutscher C.F., 1994, *Heat exchange effectiveness and pressure drop for air flow through perforated plates with and without crosswind*, Journal of Heat Transfer, 116 (2), pp. 391-399.
12. White M.J., Nellis G.F., Kelin S.A., Zhu W., Gianchandani Y., 2011, *An Experimentally Validated Numerical Modeling Technique for Perforated Plate Heat Exchangers*, Journal of Heat Transfer, 132 (11), pp. 1-9.
13. AL-Essa A.H., 2012, *Augmentation of heat transfer of a fin by rectangular perforations with aspect ratio of three*, International Journal of Mechanics and Application, 2 (1), pp. 7-11.
14. AL-Essa A.H., Fayez M.S. AL-Hussien, 2004, *The effect of orientation of square perforations on the heat transfer enhancement from a fin subjected to natural convection*, Heat and Mass Transfer, 40 (1), pp. 509-515.
15. Chin S.B., Foo J.J., Lai Y.L. *et al.*, 2013, *Forced convective heat transfer enhancement with perforated pin fins*, Heat Mass Trans, 49, pp. 1447-1448.
16. Schmidt E., Groeber H., Neumann K., 1971, *Heat Science* (in Serbian), Mechanical Faculty Belgrade, Yugoslavia, p. 734.
17. Linghui G., Tingwei G., Jichuan H., Tingying Z., 1996, *The Effect of the geometric parameters of a perforated plate on its heat transfer characteristics*, Cryogenics, 36 (2), pp. 443-446.
18. Sparrow E.M., Ortiz M.C., 1982, *Heat transfer coefficients for the upstream face of a perforated plate positioned normal to an oncoming flow*, International Journal of Heat and Mass Transfer, 25 (1), pp. 127-135.
19. Dorignac E., Vullierme J.J., Broussely M., Foulon C., Mokkadem M., 2005, *Experimental heat transfer on the windward surface of a perforated flat plate*, International Journal of Thermal Science, 44 (5), pp. 885-893.
20. Sparrow E.M., O'Brien J.E., 1980, *Heat transfer coefficients on the downstream face of an abrupt enlargement or inlet constriction in a pipe*, Journal of Heat Transfer, 102 (3), pp. 408-414.
21. Brunger A.P., Hollands K.G.T., Van Decker G.W.E., 2001, *Heat-exchange relations for unglazed transpired solar collectors with circular holes on a square or triangular pitch*, Solar Energy, 71 (1), pp. 33-45.
22. Rodriguez J.I., Mills A.F., 1996, *Heat transfer and flow friction characteristics of perforated-plate heat exchangers. experimental heat transfer*, Journal of Thermal Energy Generation, Transport, Storage and Conversion, 9 (4), pp. 335-356.
23. Andrew M.H., Shaaban A.H., Jamil A.K., Ian G.S., 2005, *CFD Heat Transfer Investigation into the convective Coefficient of a Perforated Plate*, Proceeding of HT2005, "ASME Summer Heat Transfer Conference", pp. 883-894.
24. Kutscher C.F., *An investigation of heat transfer for air flow through low porosity perforated plates*, Dissertation, University of Colorado at Boulder, 1992., p. 289.